Recycling of subducted Indian continental crust constrained by late Cretaceous mafic dykes in central Lhasa block of the Tibetan plateau

Lu-Lu Hao[a, b*], Andrew C. Kerr[c], Qiang Wang[a, b, d*], Lin Ma[a, b], Yue Qi[a, b], Ming Xiao[a], Quan Ou[e]

[a] State Key Laboratory of Isotope Geochemistry, Guangzhou Institute of Geochemistry, Chinese Academy of Sciences (CAS), Guangzhou 510640, China

[b] CAS Center for Excellence in Deep Earth Science, Guangzhou, 510640, China

[c] School of Earth and Environmental Sciences, Cardiff University, Cardiff, CF10 3AT, UK

[d] College of Earth and Planetary Sciences, University of CAS, Beijing 100049, China

[e] State Key Laboratory of Oil and Gas Reservoir Geology and Exploitation, Institute of Sedimentary Geology, Chengdu University of Technology, Chengdu 610059, China

*Corresponding authors:

Lu-Lu Hao (haolulu@gig.ac.cn); Qiang Wang (wqiang@gig.ac.cn)

ABSTRACT

The question of whether subducted continental crust can be recycled into post-collisional magmatism in continental collisional zones remains controversial. Post-collisional mantle-derived ultrapotassic rocks are widespread in western part of central Lhasa block (WCL) of the Tibet-Himalaya orogen and show arc-type trace-element signatures and very enriched Sr-Nd isotopes, which have been explained by the recycling of subducted Indian continental crust. However, due to the lack of late Cretaceous mafic magmatism in the WCL, the nature of the ancient subcontinental lithospheric mantle (SCLM) beneath the WCL has not been well constrained. It is therefore still unclear whether the enriched components of these ultrapotassic rocks were derived from subducted Indian continental crust or inherited from the ancient SCLM. Here we report the mafic dykes from the TangraYumco area in the WCL, which formed at ~90 Ma (whole-rock ^{40}Ar-^{39}Ar, and zircon and titanite U-Pb ages). The diabase-porphyrites and diorite-porphyrites are similar to intraplate Nb-enriched basalts and magnesium adakitic rocks, respectively. This rock association reveals the lithospheric foundering process. Furthermore, the diabase-porphyrites generated by the interaction between the ancient SCLM and asthenosphere provide important constraints on the nature of the ancient SCLM, which shows distinct Nd isotopes to the post-collisional ultrapotassic rocks. In addition, the NW Lhasa block was in a rear-arc environment since the late Cretaceous and thus this SCLM was not significantly influenced by the ongoing northward subduction of the Indus-YarlungZangbu Neo-Tethys ocean. Finally, we propose that the post-collisional ultrapotassic rocks cannot be sourced from the ancient SCLM, but instead were derived from a relatively depleted mantle (e.g., juvenile lithospheric mantle) metasomatized by subducted Indian continental crust. Thus, this study confirms the recycling of subducted continental materials in continental collisional orogens.

Keywords: lithosphere-asthenosphere interaction; late Cretaceous mafic dykes; adakitic rocks; Tibetan plateau; Indian continental subduction; crustal recycling

1. Introduction

Subduction zones are the primary locations where mass and energy are exchanged between the mantle and crust (e.g., Elliott, 2004; Tatsumi, 2005). Recycling of oceanic lithospheric materials in oceanic subduction zones has been widely studied and understood. The oceanic subduction factory processes raw materials (e.g., oceanic sediments and oceanic crust) and manufactures arc magmas as products. However, recycling of continental crust materials into the deep mantle by subduction in continental subduction zones is much less studied, and it remains unclear whether subducted continental crust can be recycled into post-collisional magmatism (e.g., Ducea, 2016).

The Himalaya-southern Tibet collisional orogen formed during the early Cenozoic and is widely recognized as one of the most outstanding natural laboratories for studying continental subduction (Yin and Harrison, 2000; Tapponnier et al., 2001). The Lhasa block (the southernmost edge of the Tibetan plateau) includes abundant post-collisional mafic igneous rocks (i.e., ultrapotassic rocks) (e.g., Guo et al., 2019; Yakovlev et al., 2019). These ultrapotassic rocks provide unique insights into the compositions of the deep mantle and its thermal characteristics during the post-collisional stage (Liu et al., 2011) and have important implications for understanding Indian continental subduction (e.g., Chung et al., 2005; Hao et al., 2018, 2022). These rocks are characterized by arc-type trace-element distribution patterns and markedly enriched Pb-Nd-Sr isotope compositions, and many studies have proposed that they have been derived from a mantle source metasomatized by subducted Indian continental crust (Ding et al., 2003; Zhao et al., 2009; Guo et al., 2013). However, this genetic model has not been widely accepted (e.g., Mahéo et al., 2009; Liu et al., 2015; Hao et al., 2022). The ultrapotassic rocks generally occur in the western part of central Lhasa block (WCL), which is considered to be a microcontinent underlain by an ancient SCLM (subcontinental lithospheric mantle) (Zhu et al., 2013; Wang et al., 2018). Such a SCLM could have evolved due to the oceanic subduction during the Mesozoic. However, due to the lack of late Cretaceous mafic rocks in the WCL, the nature of this ancient SCLM during ~90 Ma has not been well constrained. Lei et al. (2022) recently identified ~90 Ma gabbroic rocks from the Taruocuo area in the WLB, yet these rocks were considered to be derived from a metasomatized asthenosphere mantle, i.e., a juvenile lithospheric mantle formed during prior oceanic subduction. Thus, it is still unclear whether the enriched components of the post-collisional ultrapotassic rocks were derived from subducted Indian continental crust or inherited from the ancient SCLM beneath the WCL. This significantly hinders our understanding of the recycling of subducted continental crust materials in this typical continental collisional zone.

The late Cretaceous (~90 Ma) magmatism is intensive in the NW Lhasa block but dominated by intermediate-felsic igneous rocks. The mafic rocks are poorly studied, which limits the constraints on not only the nature of the ancient SCLM beneath the WLB but also the geodynamic processes responsible for this period of magmatism. For example, Ma and Yue (2010) ascribed this magmatism to the northward subduction of the Indus-YarlungZangbu Neo-Tethys oceanic slab. However, many recent studies based on the occurrence of adakitic rocks (Sun et al., 2015; Lei et al., 2020) and magnesian andesite-dacites (Wang et al., 2014) suggested that the late Cretaceous magmatism in the NW Lhasa block should be induced by the delamination of the thickened lithosphere after Lhasa-Qiangtang collision during the early Cretaceous (Kapp et al., 2007; Zhu et al., 2016; Hao et al., 2019b). However, in this model the interaction between the upwelling asthenosphere and surrounding lithospheric mantle which commonly occurred during the lithospheric delamination, has not yet been identified in this area.

In this contribution, we study the late Cretaceous (~90 Ma) mafic dykes (including diabase-porphyrite and diorite-porphyrite) from the TangraYumco area in central Lhasa block. Integrated studies of major, trace element, and Sr-Nd-Hf isotopes reveal that diabase-porphyrite and diorite-porphyrite dykes have some affinities of intra-plate Nb-enriched basalts and magnesium adakitic rocks, respectively. Such a rock association indicate the lithospheric foundering. Moreover, the diabase-porphyrites are shown to be generated by the interaction between the asthenosphere and an ancient SCLM, which thus could provide important constraints on the nature of the ancient SCLM. A comparison of Sr-Nd isotopes between the post-collisional ultrapotassic rocks in the Lhasa block and the ~90 Ma ancient SCLM suggested that the former should originate from a juvenile lithospheric mantle metasomatized by subducted Indian continental slab, rather than from the ancient SCLM.

2. Geological Background and Samples

South-to-north, the Himalayan-Tibetan orogen is composed of the Himalaya, Lhasa, Qiangtang, and Songpan-Ganze blocks, which are separated by the Indus-YarlungZangbu, Bangong-Nujiang, and Jinsha suture zones, respectively (Fig. 1) (Yin and Harrison, 2000). The closure of the Bangong-Nujiang Tethys ocean (BNTO) (leading to the Bangong-Nujiang suture zone, BNSZ) took place no later than the late Cretaceous (~100 Ma) (Zhu et al., 2016; Hao et al., 2019b). The northward subduction of the Indus-YarlungZangbu Neo-Tethys oceanic slab (IYZTO) occurred during the Mesozoic and its closure (leading to the Indus-YarlungZangbu suture zone, IYZSZ) happened in the early Cenozoic (Zhu et al., 2013). The Lhasa block can be divided into southern, central, and northern Lhasa sub-blocks (SL, CL, NL) by the Luobadui-Milashan fault (LMF) and Shiquanhe-NamTso mélange zone (SNMZ), respectively (Fig. 1) (Zhu et al., 2013). The central Lhasa sub-block is considered to be a microcontinent comprising ancient lithospheric mantle and crust, whereas the northern and southern Lhasa sub-blocks have been interpreted as accreted arcs produced by southward subduction of the BNTO and northward subduction of the ITZTO, respectively (Zhu et al., 2011; Wang et al., 2018).

After the initial collision between India and Eurasia (Himalaya-Lhasa), the ongoing syn-collision (the Indian continental plate was still being dragged by subducted IYZTO slab), induced the breakoff of the oceanic slab from the continental plate at ~50-45 Ma (e.g., Ji et al., 2016; Zhu et al., 2015). The collision zone then evolved into a post-collisional intra-continent setting (e.g., Mo et al., 2007). Cenozoic post-collisional igneous rocks are widespread in the Lhasa block and mainly consist of ultrapotassic, high-silica potassic, and felsic adakitic rocks (e.g., Hao et al., 2019a). The high-silica potassic and felsic adakitic rocks were generally considered to originate from the reworking of the lower crust beneath the Lhasa block (Hou et al., 2004; Hao et al., 2019a; Zhang et al., 2022). The ultrapotassic rocks were widely suggested to be derived from an enriched mantle source metasomatized by subducted Indian continental slab, given their very enriched Sr-Nd-Pb isotope signatures. However, they mainly occur in the western part of central Lhasa block (WCL) (Liu et al., 2014), which likely has an ancient and enriched SCLM. The possibility that these enriched Sr-Nd isotope signatures likely originated from the ancient SCLM cannot be fully ruled out.

Here we focus on the late Cretaceous mafic dykes in the TangraYumco area (Fig. 2-3) to clarify the nature of the ancient SLCM then. In this area, there are Carboniferous, Permian, Triassic, Jurassic, Cretaceous, and Cenozoic strata and the magmatic rocks mainly include Mesozoic-Paleocene granitoids and volcanic rocks, and Miocene post-collisional K-rich rocks. We collect the diabase-porphyrite dykes from the Yaqian and Ningguo villages and diorite-porphyrite dykes from the Daguo village (Fig. 2). Significantly, the mafic dykes are spatially closed with the post-collisional ultrapotassic rocks. The diorite-porphyrite rocks mainly comprise phenocrysts of plagioclase and amphibole set in a groundmass of amphibole, plagioclase and quartz (Fig. 3e). The diabase-porphyrite rocks have plagioclase and amphibole as phenocrysts (Fig. 3f). The groundmass has ophitic texture with (sub)euhedral plagioclase and anhedral clinopyroxene and amphibole.

3. Analytical Methods and Results

Whole-rock major- and trace-elemental and Sr-Nd isotope analyses were conducted at the State Key Laboratory of Isotope Geochemistry, Guangzhou Institute of Geochemistry (GIG), Chinese Academy of Sciences (CAS), Guangzhou. Bulk-rock $^{40}Ar/^{39}Ar$ dating was conducted at the Analytical Laboratory of Beijing Research Institute of Uranium Geology (BRIUG). Zircon and titanite U-Pb dating was conducted at the state Key Laboratory of Lithospheric Evolution, Institute of Geology and Geophysics (IGG), CAS, Beijing. Zircon Hf isotope measurements were performed at the Nanjing Hongchuang Geological Exploration Technology Service Co. Ltd. The detailed discussions of the methodology and analytical results can be found in the Appendix.

3.1 Ages

Four diabase-porphyrite samples (QT32-5 and QT32-6 from Yaqian, NG01-1 and NG01-2 from Ningguo) were selected for $^{40}Ar/^{39}Ar$ dating (Fig. 4). Each sample gives a consistent plateau age and isochron age. Specifically, the Yaqian sample QT32-5 yields whole-rock $^{40}Ar/^{39}Ar$ weighted mean and normal isochron ages of 90.1± 1.1 and 91.1± 1.4 Ma, respectively (Fig. 4a). Sample QT32-6 gives whole-rock $^{40}Ar/^{39}Ar$ weighted mean and normal isochron ages of 92.1± 1.0 and 93.8± 1.1 Ma, respectively (Fig. 4b). The Ningguo samples NG01-1 and NG01-2 yield whole-rock $^{40}Ar/^{39}Ar$ weighted mean ages of 88.0± 0.9 and 85.4± 1.3 Ma, respectively, consistent with their corresponding normal isochron ages (87.0± 1.9, 88.1± 2.8 Ma, respectively) (Fig. 4c-d). Thus, we conclude that the TangraYumco diabase-porphyrites were emplaced in the late Cretaceous (ca. 92-85 Ma).

Three diorite-porphyrite samples from Daguo (ZB105-1, ZB106-1, and ZB107-1) were selected for LA-ICP-MS zircon U-Pb dating. They all yield concordant $^{206}Pb/^{238}U$ ages with weighted mean ages of 88.3± 2.6, 84.4± 2.2, and 85.4± 1.3 Ma, respectively (Fig. 5a-c). Titanite grains from sample ZB107-1 also yield a lower intercept age of 87.6± 1.8 Ma on a Tera-Wasserburg diagram (mean square of weighted deviates = 2.9) (Fig. 5d). Collectively, the TangraYumco diorite-porphyrites were formed at ca. 86 Ma (late Cretaceous), coeval with the diabase-porphyrites in this area.

3.2 Major and Trace Element

The diabase-porphyrites have relatively low SiO_2 (45.4-51.5 wt.%), MgO (5.1-8.1 wt.%), and TiO_2 (1.1-1.5 wt.%) contents. They show variable Mg# [$Mg^{2+}/(Fe^{2+}+Mg^{2+})$] (54-64) values, and Cr (78-489 ppm) and Ni (58-241 ppm) contents. They have variable and high loss on ignition values (LOI) of 1.4-9.0 wt.%, indicating that some samples could have been altered. Potential element mobility in altered igneous rocks limits the use of standard classification diagrams like total alkali-silica (TAS) and K_2O vs. SiO_2. Alternatively, we employ a plot of Co versus Th (Hastie et al., 2007) to show their basaltic affinities (Fig. 6a). On a chondrite-normalized REE (rare earth element) plot (Fig. 6c), they are characterized by enrichment of light REE (LREEs) and depletion of heavy REEs (HREEs) with normalized La/Yb values $(La/Yb)_N$ of 7.8-16.1, and negligible Eu anomalies (Eu/Eu* = 0.86-0.98). They show subparallel primitive mantle-normalized trace-element patterns but with more-variable large ion lithophile elements (LILEs, e.g., Rb, Ba) (Fig. 6d). These diabase-porphyrites exhibit some arc-like geochemical features, e.g., enrichment of LILEs, depletion of HREEs and high field strength elements (HFSEs, e.g., Nb, Ta), and positive Pb anomalies. However, compared to normal arc basalts, they contain more Nb (8.0-16.4 ppm) and Zr (115-217 ppm), similar to Nb-enriched arc basalts (Nb contents of 5-20 ppm, Hastie et al., 2011). In a plot of Zr vs. Zr/Y, they classify as within-plate basalts (Fig. 7a). Additionally, these rocks exhibit distinctly lower Zr/Nb ratios than subduction zone lavas (Fig. 7b). These geochemical features are very similar to those of the Gaoligong Eocene basaltic dykes in the SE Tibetan plateau (Xu et al., 2008) (Fig. 7b). The latter is considered to be derived from the interaction between the lithospheric mantle and asthenosphere (Xu et al., 2008).

The diorite-porphyrites are relatively fresh and have low LOI (0.7-1.4 wt.%) contents. They have high SiO_2 (60.3-62.4 wt.%) but low total-alkaline (Na_2O+ K_2O) (6.2-6.7 wt.%) contents, and are sub-alkaline (Fig. 6b). They have relatively high MgO (2.5-3.4 wt.%) and Ni (32-43 ppm) contents, and Mg# (49-53) values. They show significant fractionation between LREEs and HREEs with $(La/Yb)_N$ = 19.6-35.5 and weakly negative Eu anomalies (Eu/Eu* = 0.78-0.89) (Fig. 6c). Their primitive mantle-normalized trace-element distribution patterns are characterized by enrichment of LILEs and Pb, depletion of HREEs and HFSEs, and no Sr anomalies (Fig. 6d). They have high Sr (656-753 ppm) but low Y (13.8-15.3 ppm) and Yb (1.15-1.33 ppm) contents, and thus high Sr/Y (45-53) and La/Yb (27-50) ratios (Fig. 8a-b). These geochemical features, combined with their high Al_2O_3 (16.1-15.8 wt.%; > 15.0 wt.%) contents indicate their close adakitic affinity (Castillo, 2012).

3.3 Sr-Nd-Hf Isotopes

The diabase-porphyrites have a wide range of initial $^{87}Sr/^{86}Sr$ values (0.7082-0.7108), initial $^{143}Nd/^{144}Nd$ ratios (0.512116-0.512345) and initial εNd values [εNd(t)] of -7.92 to -3.45 (Fig. 9a). The diorite-porphyrites have relatively uniform Sr-Nd isotopes ($^{87}Sr/^{86}Sr(i)$ = 0.7090-0.7092, $^{143}Nd/^{144}Nd(t)$ = 0.512200-0.512217, and εNd(t) = -6.28 to -5.95, Fig. 9a).

The Hf isotopes of zircon grains were analyzed in the same domains where the U-Pb ages were determined. A total of 27 syn-magmatic zircon grains from three diorite-porphyrite samples were analyzed for $^{176}Hf/^{177}Hf$ isotopic ratios (Fig. 9b). These three samples yield similar and overlapped zircon εHf(t) values. Specifically, zircons of sample ZB105-1 yield initial $^{176}Hf/^{177}Hf$ ratios of 0.282538-0.282568, corresponding to εHf(t=86 Ma) values of -6.37 to -5.31. The zircons from sample ZB106-1 give $^{176}Hf/^{177}Hf(t)$ and εHf(t) values of 0.282562-0.282603 and -5.55 to -4.10, respectively. Analyses of zircons from sample ZB107-1 show $^{176}Hf/^{177}Hf(t)$ ratios of 0.282557-0.282616, which correspond to εHf(t) values of -5.71 to -3.62. Collectively, the diorite-porphyrites have enriched zircon Hf isotope compositions with εHf(t) = -6.37 to -3.62 (Fig. 9b), overlapping with the coeval (~88 Ma) Coqen granites (εHf(t)= -11 to -4) in the WLB (Lei et al., 2020).

4. Discussion

4.1 Petrogenesis of Diabase-porphyrite Dykes

4.1.1 Alteration, Fractional crystallization and Crustal Contamination

Many LILEs are mobilized during weathering, hydrothermal, and low-grade metamorphism (e.g., Pearce, 2014). Thus, the alteration effects on elemental mobility should be assessed before discussing the geochemical data. Representative variation diagrams for the diabase-porphyrites are presented, plotting incompatible elements against immobile Nb (Fig. DR1). On log-log plots, positive linear vectors should form if the elements are immobile (e.g., Hastie et al., 2011). The bivariate diagram of Ba vs. Nb shows a large scatter without a pre-alteration positive linear trend, indicating Ba is mobile (Fig. DR1a).

Conversely, elements including Rb, Pb, and Sr in most samples have tight correlations with Nb, suggesting their immobility (Fig. DR1b-d). Furthermore, contents and isotope ratios of Sr show no systematic correlations with increasing LOI contents (Fig. DR1e-f). Thus, these values can be used to discuss the genesis of the diabase-porphyrites.

La/Sm ratios of the diabase-porphyrites show a positive correlation with La contents (Fig. 10a), suggesting that partial melting and source compositions are more important than fractional crystallization. The correlation between CaO/Al_2O_3 ratios and MgO is insignificant (Fig. 10b), indicating negligible clinopyroxene fractionation. Besides, the weakly negative Eu anomalies remain nearly constant with decreasing MgO (Fig. 10c), arguing against significant plagioclase fractionation during magma evolution. However, a positive correlation between MgO and Ni contents (Fig. 10d) indicates minor olivine fractionation.

Mantle-derived mafic magmas can experience crustal contamination when they rise from their mantle sources through the continental crust. A negative correlation between SiO_2 and εNd and a positive correlation between Nb/La and εNd (Fig. 11a-b) appear to be consistent with crustal contamination. However, the continental crust generally has low Sm/Nd and MgO values (Xu et al., 2008). Thus, it is expected that the most contaminated samples (with lowest εNd) should also have the lowest Sm/Nd and MgO. These trends have not been observed in the TangraYumco diabase-porphyrites (Fig. 11c-d). Therefore, crustal contamination cannot adequately explain their geochemical compositions. Notably, these diabase-porphyrites have broadly similar Nb/La ratios regardless of MgO and SiO_2 contents (Fig. 11e-f). This suggests that negative Nb-Ta anomalies in the diabase-porphyrites are derived from the mantle sources rather than the crustal contamination.

Conclusively, the TangraYumco diabase-porphyrite dykes were generated by partial melting of a mantle source and experienced insignificant fractional crystallization, crustal contamination, or post-emplacement alteration.

4.1.2 Diabase-porphyrites Generated by Lithosphere Mantle-Asthenosphere Interaction

As discussed above, the TangraYumco diabase-porphyrites exhibit high Zr and Nb contents and Zr/Y and Nb/Zr ratios and thus have a similar composition to Nb-enriched and intra-plate basalts. They were most likely connected to the asthenospheric upwelling rather than oceanic subduction (Xu et al., 2008). However, the TangraYumco diabase-porphyrites have well-developed Nb-Ta depletions, enriched Sr-Nd isotopes, and arc-like features (e.g., Pb enrichment). Having already ruled out crustal assimilation, a contribution from a metasomatized lithospheric mantle may explain the compositions of these rocks. The lithospheric mantle can preserve various geochemical heterogeneities generated by prior oceanic or continental subduction and typically displays enriched and fertile geochemical signatures (Tang et al., 2012). The ~90 Ma gabbroic rocks from the Taruocuo area in the WLB were considered to be derived from a juvenile lithospheric mantle (Lei et al., 2022). Such a mantle domain does not significantly contribute to the formation of the TangraYumco diabase-porphyrites given that the former has more depleted Sr-Nd isotopes than the latter (Fig. 9a). Instead, the arc-like geochemical characteristics of the diabase-porphyrites originate from an ancient and fertile lithospheric mantle beneath the WLB. The positive correlation between Nb/La and Nd isotope compositions (Fig. 11a) can be accorded for by the source mixing between such a SCLM and the asthenospheric mantle. The range in Sr-Nd isotope signatures of the diabase-porphyrites indicate variable contamination by the lithospheric mantle with the samples plotting on a mixing curve between the sample NG01-2 and the N-MORB (Fig. 9a). NG01-2 can be considered as an end-member that represents the isotopic composition of the ancient SCLM beneath the WLB.

4.2 Petrogenesis of Diorite-porphyrite Dykes: Partial Melting of Delaminated Lower Crust

As shown above, the TangraYumco diorite-porphyrites show close adakitic affinity. A range of genetic models for the formation of adakitic rocks have been proposed, e.g., high-pressure fractional crystallization from the basaltic magmas (Macpherson et al., 2006); partial melting of subducted oceanic slab (Defant and Drummond, 1990), thickened (Chung et al., 2003) or delaminated (Xu et al., 2002) lower continental crust.

Adakitic rocks formed by high-pressure fractional crystallization of garnet from basaltic magmas usually display a positive trend on a Dy/Yb (or La/Yb) versus SiO_2 diagram (Macpherson et al., 2006), which is not the case for the TangraYumco diorite-porphyrites (Fig. 8c). In addition, the TangraYumco diorite-porphyrites have enriched Sr-Nd isotopes, arguing against their derivation from an oceanic slab. Their isotopic signatures are also distinct from those of these juvenile crust-derived adakitic rocks (e.g., Azhang and Gaerqiong) in the WLB (Sun et al., 2015; Lei et al., 2020) (Fig. 9a). Instead, their Sr-Nd and zircon Hf isotope compositions are similar to those of the early Cretaceous ancient crust-derived felsic rocks (Fig. 9a) (Wang et al., 2018; Lei et al., 2020). Furthermore, they have relatively high MgO and Ni contents and Mg# (> 49) values, which are higher than the lower crust-derived adakitic rocks (e.g., Azhang), but similar to the coeval Zhuogapu magnesian andesite-dacites (Fig. 8d-e). They appear to be most similar to delaminated lower crust-derived adakites rather than thick lower crust-derived adakites (Fig. 8d). Thus, we suggest that the TangraYumco diorite-porphyrites were most likely generated by partial melting of the delaminated, thickened ancient lower crust beneath the WLB. Lei et al. (2020) proposed crustal thickening of the NW Lhasa block during 110-90 Ma. At ~90 Ma the crust is likely to have reached a > 50 km thickness, and can be delaminated into the asthenosphere (Gao et al., 2004).

4.3 Late Cretaceous Lithospheric Delamination in NW Lhasa Block

Previous studies have shown the intensive magmatism in the SE Lhasa block (e.g., Milin-

Langxian areas) during the late Cretaceous (Fig. 1). These magmatic rocks contain substantial basaltic rocks (e.g., Ma et al., 2013). They occurred near the Indus-YarlungZangbu suture zone and their generation was widely considered to be related to the northward subduction of the Neo-Tethys ocean, though the detailed geodynamic settings remain highly debated (e.g., oceanic ridge subduction, oceanic slab roll-back).

This study combined with literature data revealed that the coeval (late Cretaceous) magmatism also intensively developed in the NW Lhasa block (Fig. 1). These magmatic rocks, different from those in the SE Lhasa block, are dominated by intermediate-felsic rocks with minor basaltic rocks. The intermediate-felsic rocks contain low-Mg# adakitic rocks (Sun et al., 2015), magnesian adakitic rocks (Chen et al., 2015; this study), and magnesian but non-adakitic rocks (Wang et al., 2014), which are related to partial melting of the lower crust or delaminated lower crust. The basaltic rocks were generated by partial melting of a juvenile SCLM (Lei et al., 2022) or by the interaction between the asthenosphere and an ancient SCLM (this study). The magmatism is far away from the Indus-YarlungZangbu suture zone but instead distributed in central and northern Lhasa sub-blocks. Given such differences in magmatism between the NW and SE Lhasa, we suggested that the magmatism in the NW Lhasa block should not be linked to the Neo-Tethys oceanic subduction. Alternatively, such rock associations in the NW Lhasa block can be readily reconciled with a geodynamic model whereby a thickened lithosphere foundered into the asthenosphere mantle (Fig. 12). During the lithospheric delamination, the available space would have been filled by the hot, rising asthenospheric mantle. The hot mantle triggered melting in the overlying domains (i.e., the remaining lithospheric mantle, and the lower crust) (Turner et al., 1992). In the case of the NW Lhasa block, given the occurrence of delaminated lower crust-derived adakitic rocks, we suggested that the lithospheric mantle and partial lower crust could sink into the asthenosphere mantle (Fig. 12). The interactions between the lithospheric mantle and asthenosphere, and between the delaminated lower crust-derived melts and mantle peridotite produced the diabase-porphyrites and diorite-porphyrites, respectively (Fig. 12).

4.4 Implication for Recycling of Subducted Indian Continental Crust

Cenozoic post-collisional ultrapotassic rocks are widespread in the WCL and are probably derived from a mantle source enriched by Indian continental subduction and thus record the recycling of subducted Indian continental crustal materials (Ding et al., 2003; DeCelles et al., 2011). However, the possibility that the enriched geochemical features of the ultrapotassic rocks were inherited from the ancient SCLM beneath the WLB cannot be fully ruled out. This hinders our understanding of the recycling of subducted Indian continental materials in the Himalaya-Tibet collisional orogen.

This study identifies the late Cretaceous diabase-porphyrite dykes in the WCL that were generated by the interaction between asthenospheric and ancient lithospheric mantle. Thus, they can provide important constraints on the nature of the ancient SCLM beneath the WCL. In a Sr-Nd isotope plot (Fig. 9a), the diabase-porphyrites form a trend extending from the depleted asthenospheric mantle to an enriched SCLM. Moreover, since the late Cretaceous the NW Lhasa block was no longer affected by the BNTO and in a rear-arc (refer to IYZTO) environment. So, this ancient SCLM can be independent of the oceanic subduction and preserve its geochemical features, until the beginning of the Indian continental subduction. Though the late Cretaceous ancient SCLM shows similar Sr isotope ratios to post-collisional primitive ultrapotassic rocks (i.e., the Konglong ultrapotassic enclaves, Hao et al., 2018), the SCLM has less enriched Nd isotopes than the ultrapotassic rocks. Thus, it is unlikely that the post-collisional ultrapotassic rocks were derived from the ancient SCLM, let alone an ancient SCLM metasomatized by the subducted Indian continental crust, which would have more enriched Sr-Nd isotopes (Fig. 9a). Instead, we suggest that the post-collisional ultrapotassic rocks were derived from a relatively depleted mantle (e.g., juvenile lithospheric mantle formed during prior oceanic subduction) metasomatized by subducted Indian continental crust. Simple mixing modeling between the two end-members of the juvenile lithospheric mantle (Lei et al., 2022) beneath the WCL and the Indian continental crust (Guo et al., 2013) can well reproduce the Sr-Nd isotopes of the post-collisional ultrapotassic rocks (Fig. 9a). This study therefore confirms the recycling of subducted continental materials during Indian continental subduction, and so can promote our understanding of other continental collisional zones on Earth.

5. Conclusions

The TangraYumco diabase-porphyrite and diorite-porphyrite dykes in central Lhasa block of southern Tibet were generated at ~90 Ma, and show close affinity to intra-plate, Nb-enriched basalts and adakitic rocks, respectively. The diabase-porphyrites were produced by the interaction between the ancient lithospheric mantle and asthenosphere, and the diorite-porphyrites were generated by partial melting of the delaminated, thickened lower continental crust. The diabase-porphyrites constrain the nature of the latest pre-collisional ancient sub-continental lithospheric mantle (SCLM) beneath the WLB. The post-collisional ultrapotassic rocks show different Nd isotopes to the ancient SCLM, and should be derived from the juvenile lithospheric mantle metasomatized by subducted Indian continental crust. This study therefore confirms the recycling of subducted continental materials in continental collisional orogens.

Acknowledgements

This study is financially supported by the National Natural Science Foundation of China (NSFC) (41802048, 42021002, 42073025), Youth Innovation Promotion Association CAS (2022357), and the Second Tibetan Plateau Scientific Expedition and Research (STEP) (2019QZKK0702). This is contribution No.IS-xxxx from GIGCAS.

References

Castillo, P.R., 2012, Adakite petrogenesis: Lithos, 134-135, 304-316.

Chen, J.L., Xu, J.F., Yu, H.X., Wang, B.D., Wu, J.B., Feng, Y.X., 2015. Early late Cretaceous high-Mg# granitoids in southern Tibet: Implications for the early crustal thickening and tectonic evolution of the Tibetan Plateau. Lithos, 232, 12-22.

Chung, S.L., Liu, D.Y., Ji, J.Q., Chu, M.F., Lee, H.Y., Wen, D.J., Lo, C.H., Lee, T.Y., Qian, Q., Zhang, Q., 2003, Adakites from continental collision zones: Melting of thickened lower crust beneath southern Tibet: Geology, 31, 1021-1024.

Chung, S.L., Chu, M.-F., Zhang, Y., Xie, Y., Lo, C.-H., Lee, T.-Y., et al. (2005). Tibetan tectonic evolution inferred from spatial and temporal variations in post-collisional magmatism. Earth Science Reviews, 68(3-4), 173-196.

DeCelles, P., Kapp, P., Quade, J., Gehrels, G., 2011, The Oligocene-Miocene Kailas Basin, southwestern Tibet: Record of post-collisional upper plate extension in the Indus-Yarlung suture zone. Geological Society of America Bulletin, 123, 1337-1362.

Defant, M.J., Drummond, M.S., 1990. Derivation of some modern arc magmas by melting of young subducted lithosphere: Nature, 347, 662-665.

Ding, L., Kapp, P., Zhong, D.L., Deng, W.M. (2003). Cenozoic volcanism in Tibet: Evidence for a transition from oceanic to continental subduction. Journal of Petrology, 44(10), 1833-1865.

Ducea, M., 2016. RESEARCH FOCUS: Understanding continental subduction: a work in progress. Geology, 44 (3), 239-240.

Elliott, T., 2004. Tracers of the Slab. Geophysical Monograph, 138, 23-45.

Gao, S., Rudnick, R.L., Yuan, H.L., Liu, X.M., Liu, Y.S., Xu, W.L., Ling, W.L., Ayers, J., Wang, X.C., Wang, Q.H. (2004). Recycling lower continental crust in the North China craton. Nature, 432, 892-897.

Guo, Z.F., Wilson, M., 2019. Late Oligocene-early Miocene transformation of postcollisional magmatism in Tibet. Geology, 47, 776-780.

Guo, Z.F., Wilson, M., Zhang, M.L., Cheng, Z.H., Zhang, L.H., 2013. Post-collisional, K-rich mafic magmatism in south Tibet: constraints on Indian slab-to-wedge transport processes and plateau uplift. Contrib. Mineral. Petrol., 165, 1311-1340.

Hao, L.-L., Wang, Q., Kerr, A.C., Wei, G-J., Huang, F., Zhang, M-Y., Qi, Y., Ma, L., Chen, X-F., Yang, Y-N., 2022. Contribution of continental subduction to very light B isotope signatures in post-collisional magmas: evidence from southern Tibetan ultrapotassic rocks. Earth and Planetary Science Letters, 584, 117508.

Hao, L.-L., Wang, Q., Wyman, D., Qi, Y., Ma, L., Huang, F., Zhang, L., Xia, X., Ou, Q., 2018, First identification of mafic igneous enclaves in Miocene lavas of southern Tibet with implications for Indian continental subduction. Geophysical Research Letters, 45, 8205-8213.

Hao, L.-L., Wang, Q., Wyman, D.A., Yang, J.-H., Huang, F., Ma, L., 2019a. Crust-mantle mixing and crustal reworking of southern Tibet during Indian continental subduction: evidence from Miocene high-silica potassic rocks in central Lhasa block. Lithos, 342-343, 407-419.

Hao, L.-L., Wang, Q., Zhang, C.-F., Ou, Q., Yang, J.-H., Dan, W., Jiang, Z.-Q., 2019b. Oceanic plateau subduction during closure of the Bangong-Nujiang Tethyan Ocean: Insights from central Tibetan volcanic rocks. Geological Society of America Bulletin, 131(5-6): 864-880.

Hastie, A.R., Kerr, A.C., Pearce, J.A., Mitchell, S.F., 2007. Classification of altered volcanic island arc rocks using immobile trace elements: development of the Th-Co discrimination diagram. Journal of Petrology, 48, 2341-2357.

Hastie, A.R., Mitchell, S.F., Kerr, A.C., Minifie, M.J., Millar, I.L., 2011. Geochemistry of rare high-Nb basalt lavas: Are they derived from a mantle wedge metasomatised by slab melts? Geochimica et Cosmochimica Acta, 75, 17, 5049-5072.

Hou, Z.Q., Gao, Y.F., Qu, X.M., Rui, Z.Y., Mo, X.X., 2004. Origin of adakitic intrusives generated during mid-Miocene east-west extension in southern Tibet. Earth Planet. Sci. Lett., 220, 139-155.

Huang, F., Chen, J., Xu, J., Wang, B., Li, J. (2015). Os-Nd-Sr isotopes in Miocene ultrapotassic rocks of southern Tibet: Partial melting of a pyroxenite-bearing lithospheric mantle? Geochim Cosmochim Ac, 163, 279-298.

Ji, W.Q., Wu, F.Y., Chung, S.L., Wang, X.C., Liu, C.Z., Li, Q.L., et al. (2016). Eocene neo-Tethyan slab breakoff constrained by 45 Ma oceanic island basalt-type magmatism in southern Tibet. Geology, 44(4), 283-286.

Kapp, P., DeCelles, P.G., Gehrels, G.E., Heizler, M., Ding, L., 2007. Geological records of the Lhasa-Qiangtang and Indo-Asian collisions in the Nima area of central Tibet. GSA Bulletin, 119, 917-932.

Lei, M., Chen, J., Luo, Y., Wang, D., 2022. Nature of the Late Cretaceous mantle source beneath the western Lhasa terrane, southern Tibet: Insights from the newly discovered mafic intrusion. Lithos, 420-421, 106721.

Lei, M., Chen, J-L., Xu, J-F., Zeng, Y-C., Xiong, Q-W., 2020. Late Cretaceous magmatism in the NW Lhasa Terrane, southern Tibet: Implications for crustal thickening and initial surface uplift. GSA Bulletin, 132(1-2): 334–352.

Liu, C.Z., Wu, F.Y., Chung, S.L., Zhao, Z.D. (2011). Fragments of hot and metasomatized mantle lithosphere in Middle Miocene ultrapotassic lavas, southern Tibet. Geology, 39(10), 923-926.

Liu, D., Zhao, Z., Zhu, D., Niu, Y., Depaolo, D.J., Harrison, T.M., et al. (2014). Postcollisional potassic and ultrapotassic rocks in southern Tibet: Mantle and crustal origins in response to India-Asia collision and convergence. Geochim Cosmochim Ac, 143, 207-231.

Liu, D., Zhao, Z., Zhu, D., Niu, Y., Widom, E., Teng, F., et al. (2015). Identifying mantle carbonatite metasomatism through Os-Sr-Mg isotopes in Tibetan ultrapotassic rocks. Earth and Planetary Science Letters, 458-469.

Ma, G-L., Yue, Y-H., 2010. Cretaceous volcanic rocks in northern Lhasa Block: constraints on the tectonic evolution of the Gangdise Arc. Acta Petrologica et Mineralogica, 29(5), 525-538.

Ma, L., Wang, Q., Wyman, D., Li, Z-X., Jiang, Z-Q., Yang, J-H., Gou, G-N., Guo, H-F., 2013. Late Cretaceous (100–89 Ma) magnesian charnockites with adakitic affinities in the Milin area, eastern Gangdese: Partial melting of subducted oceanic crust and implications for crustal growth in southern Tibet. Lithos, 175-176, 315-332.

Macpherson, C.G., Dreher, S.T., Thirlwall, M.F., 2006. Adakites without slab melting: High pressure differentiation of island arc magma, Mindanao, the Philippines: Earth and Planetary Science Letters, 243, 581-593.

Mahéo, G., Blichert-Toft, J., Pin, C., Guillot, S., Pecher, A., 2009. Partial melting of mantle and crustal sources beneath south Karakorum, Pakistan: Implications for the Miocene geodynamic evolution of the India-Asia Convergence Zone. Journal of Petrology, 50, 3, 427-449.

Mo, X., Hou, Z., Niu, Y., Dong, G., Qu, X., Zhao, Z., Yang, Z., 2007. Mantle contributions to crustal thickening during continental collision: Evidence from Cenozoic igneous rocks in southern Tibet. Lithos, 96, 1, 225-242.

Pearce, J.A., 2014. Immobile element fingerprinting of ophiolites. Elements, 10, 2, 101-108.

Sun, G.Y., Hu, X.M., Zhu, D.C., Hong, W.T., Wang, J.G., Wang, Q., 2015. Thickened juvenile lower crust-derived ~90 Ma adakitic rocks in the central Lhasa terrane, Tibet. Lithos, 224, 225-239.

Sun, S.S., McDonough, W., 1989, Chemical and isotopic systematics of oceanic basalts: Implications for mantle composition and processes, in Saunders, A.D., and Norry, M.J., eds., 1989, Magmatism in the Ocean Basins: Geological Society, London, Special Publication 42, 313-345.

Tang, G-J., Wang, Q., Wyman, D.A., Li, Z-X., Xu, Y-G., Zhao, Z-H., 2012. Metasomatized lithosphere–asthenosphere interaction during slab roll-back: Evidence from Late Carboniferous gabbros in the Luotuogou area, Central Tianshan. Lithos, 155, 67-80.

Tapponnier, P., Zhiqin, X., Roger, F., Meyer, B., Arnaud, N.O., Wittlinger, G., Jingsui, Y., 2001. Oblique stepwise rise and growth of the Tibet plateau. Science, 294, 1671-1677.

Tatsumi, 2005. The subduction factory: How it operates in the evolving Earth. GSA Today, 15(7), 4-10.

Turner, S., Sandiford, M., Foden, J., 1992. Some geodynamic and compositional constraints on postorogenic magmatism. Geology, 20, 931-934.

Wang, Q., Xu, J.F., Jian, P., Bao, Z.W., Zhao, Z.H., Li, C.F., Xiong, X.L., Ma, J.L., 2006. Petrogenesis of adakitic porphyries in an extensional tectonic setting, Dexing, South China: Implications for the genesis of porphyry copper mineralization. Journal of Petrology, 47, 119-144.

Wang, Q., Zhu, D.C., Liu, A-L., Cawood, P.A., Liu, S-A., Xia, Y., Chen, Y., Wang, H., Zhang, L-L., Zhao, Z.D., 2018. Survival of the Lhasa Terrane during its collision with Asia due to crust-mantle coupling revealed by ca. 114 Ma intrusive rocks in western Tibet. Lithos, 304-307, 200-210.

Wang, Q., Zhu, D.C., Zhao, Z.D., Liu, S.A., Chung, S.L., Li, S.M., Liu, D., Dai, J.G., Wang, L.Q., Mo, X.X., 2014. Origin of the ca. 90 Ma magnesia-rich volcanic rocks in SW Nyima, central Tibet: Products of lithospheric delamination beneath the Lhasa-Qiangtang collision zone. Lithos, 198-199, 24-37.

Xu, J.F., Shinjo, R., Defant, M.J., Wang, Q., Rapp, R.P., 2002. Origin of Mesozoic adakitic intrusive rocks in the Ningzhen area of east China: Partial melting of delaminated lower continental crust? Geology, 30, 1111-1114.

Xu, Y-G., Lan, J-B., Yang, Q-J., Huang, X-L., Qiu, H-N., 2008. Eocene break-off of the Neo-Tethyan slab as inferred from intraplate-type mafic dykes in the Gaoligong orogenic belt, eastern Tibet. Chemical Geology, 255, 439-453.

Yakovlev, P.V., Saal, A., Clark, M.K., Hong, C., Niemi, N.A., Mallick, S., 2019. The geochemistry of Tibetan lavas: Spatial and temporal relationships, tectonic links and geodynamic implications. Earth and Planetary Science Letters, 520, 115-126.

Yin, A., Harrison, T.M., 2000, Geologic evolution of the Himalayan-Tibetan orogen. Annual Review of Earth and Planetary Sciences, 28, 211-280.

Zhang, L.L., Zhu, D.C., Zhao, Z.D., Dong, G.C., Mo, X.X., Guan, Q., Liu, M., Liu, M.H., 2010. Petrogenesis of magmatism in the Baerda region of Northern Gangdese, Tibet: Constraints from geochemistry, geochronology and Sr-Nd-Hf isotopes. Acta Petrologica Sinica, 26(6), 1871-1888.

Zhang, M-Y., Hao, L.-L., Wang, Q., Qi, Y., Ma, L., 2022. B-Sr-Nd isotopes of Miocene trachyandesites in Lhasa block of southern Tibet: insights into petrogenesis and crustal reworking. Frontiers in Earth Science, 10, 953364.

Zhao, Z., Mo, X., Dilek, Y., Niu, Y., DePaolo, D., Robinson, P., et al. (2009). Geochemical and Sr-Nd-Pb-O isotopic compositions of the postcollisional ultrapotassic magmatism in SW Tibet: Petrogenesis and implications for India intra-continental subduction beneath southern Tibet. Lithos, 113(1-2), 190-212.

Zhu, D.C., Zhao, Z.D., Niu, Y., Mo, X.X., Chung, S.L., Hou, Z.Q., et al. (2011). The Lhasa terrane: Record of a microcontinent and its histories of drift and growth. Earth and Planetary Science Letters, 301(1-2), 241-255.

Zhu, D., Wang, Q., Zhao, Z., Chung, S., Cawood, P.A., Niu, Y., et al. (2015). Magmatic record of India-Asia collision. Scientific Reports, 5(1), 14,289-14,289.

Zhu, D., Zhao, Z., Niu, Y., Dilek, Y., Hou, Z., Mo, X. (2013). The origin and pre-Cenozoic evolution of the Tibetan Plateau. Gondwana Research, 23(4), 1429-1454.

Zhu, D.C., Li, S.M., Cawood, P.A., Wang, Q., Zhao, Z.D., Liu, S.A., Wang, L.Q., 2016. Assembly of the Lhasa and Qiangtang terranes in central Tibet by divergent double subduction. Lithos, 245, 7-17.

Figure Captions

Fig. 1. Geological map of southern Tibet (Lhasa block) showing the main tectonic units and Mesozoic magmatism, modified from Zhu et al. (2013). The insert shows the Lhasa block in the context of the Tibetan Plateau. Abbreviations: JSSZ= Jinsha suture zone; LSSZ= Longmuco-Shuanghu suture zone; BNSZ= Bangong-Nujiang suture zone; SNMZ= Shiquanhe-NamTso mélange zone; LMF= Luobadui-Milashan fault; IYZSZ=Indus-YarlungZangbo suture zone; STDS= South Tibet Detachment System; MCT= Main Central Thrust; MBT= Main Boundary Thrust. SL, CL, NL= southern, central, and northern Lhasa sub-blocks, respectively. The studied area is located in western part of CL.

Fig. 2. Simplified geological map of the TangraYumco-Xuruco area showing the main distribution of Mesozoic-Cenozoic magmatic rocks (after Huang et al., 2015). We collect the diabase-porphyrite dykes from Garwa and Ningguo and diorite-porphyrite dykes from Daguo.

Fig. 3. Representative field photographs and photomicrographs of the mafic dykes in the TangraYumco area. (a, b, e) for diorite-porphyrite dykes and (c, d, f) for diabase-porphyrite dykes. Amp, amphibole; Pl, plagioclase; Cpx, clinopyroxene; Qtz, quartz.

Fig. 4. (a-d) $^{40}Ar/^{39}Ar$ normal isochron ages (whole-rock) for TangraYumco diabase-porphyrites. The insert shows the corresponding plateau ages.

Fig. 5. (a-c) LA-ICPMS zircon U-Pb Concordia plots for TangraYumco diorite-porphyrites; (d) Titanite U-Pb dating for diorite-porphyrite sample ZB107-1. The insert shows the representative CL images for zircon and BSE images for titanite and the red line represents 100 um.

Fig. 6. (a) Co vs. Th; and (b) TAS diagrams for TangraYumco diabase-porphyrites and diorite-porphyrites. The Gaoligong basaltic dykes are from Xu et al. (2008). The ~90 Ma

Zhuogapu magnesian andesites-dacites and Azhang adakitic rocks in the NW Lhasa block are from Wang et al. (2014) and Sun et al. (2015), respectively. (c) Chondrite-normalized REE (rare earth element) diagram; and (d) Primitive mantle-normalized trace element distribution patterns. The normalized values are from Sun and McDonough (1989).

Fig. 7. (a) Zr/Y versus Zr; and (b) Zr/Nb vs. La/Nb plots for TangraYumco diabase-porphyrites. The base diagram is after Xu et al. (2008). WPB: within-plate basalt; IAB, VAB: subduction-related basalt.

Fig. 8. (a) Sr/Y vs Y; and (b) La/Yb vs. Yb diagrams (Castillo, 2012) showing the adakitic affinity of TangraYumco diorite-porphyrites. (c) SiO_2 vs Dy/Yb. (d) SiO_2 vs. MgO, modified after Wang et al. (2006). (e) SiO_2 vs Ni.

Fig. 9. (a) Sr-Nd isotope plot. Post-collisional ultrapotassic rocks and enclaves are from Hao et al. (2018) and references therein. Laguoco basalt (Zhang et al., 2010) is used to represent the asthenosphere-derived melt ($^{87}Sr/^{86}Sr(i)$= 0.70634, εNd(t)= 4.5, Sr= 196 ppm, Nd= 4.5 ppm). The blue curve shows mixing between Laguoco basalt and sample NG01-2. The insert shows the mixing between the relatively depleted juvenile lithospheric mantle and the subducted Indian continental crust (Guo et al., 2013), which can well reproduce the Sr-Nd isotopes of ultrapotassic rocks. (b) Zircon Hf isotope plot for diorite-porphyrites.

Fig. 10. (a) La/Sm vs La; (b) MgO vs. CaO/Al_2O_3; (c) MgO vs Eu anomalies; and (d) MgO vs Ni plots for the TangraYumco diabase-porphyrites.

Fig. 11. (a-d) εNd(t) vs. Nb/La, SiO_2, MgO, and Sm/Nd, respectively, for the TangraYumco diabase-porphyrites. (e-f) Nb/La vs SiO_2 and MgO, respectively.

Fig. 12. A schematic illustration showing lithospheric delamination beneath the central and northern Lhasa sub-blocks within the Qiangtang-Lhasa collisional zone at ~90 Ma, modified from Wang et al. (2014). Abbreviations: SNMZ= Shiquanhe-NamTso mélange

zone, BNSZ= Bangong-Nujiang suture zone, SCLM= sub-continental lithospheric mantle. ①, delaminated lower crustal melt-peridotite interaction yields TangraYumco diorite-porphyrite dykes. ②, asthenosphere-ancient SCLM interaction generates TangraYumco diabase-porphyrite dykes.

Figure 1

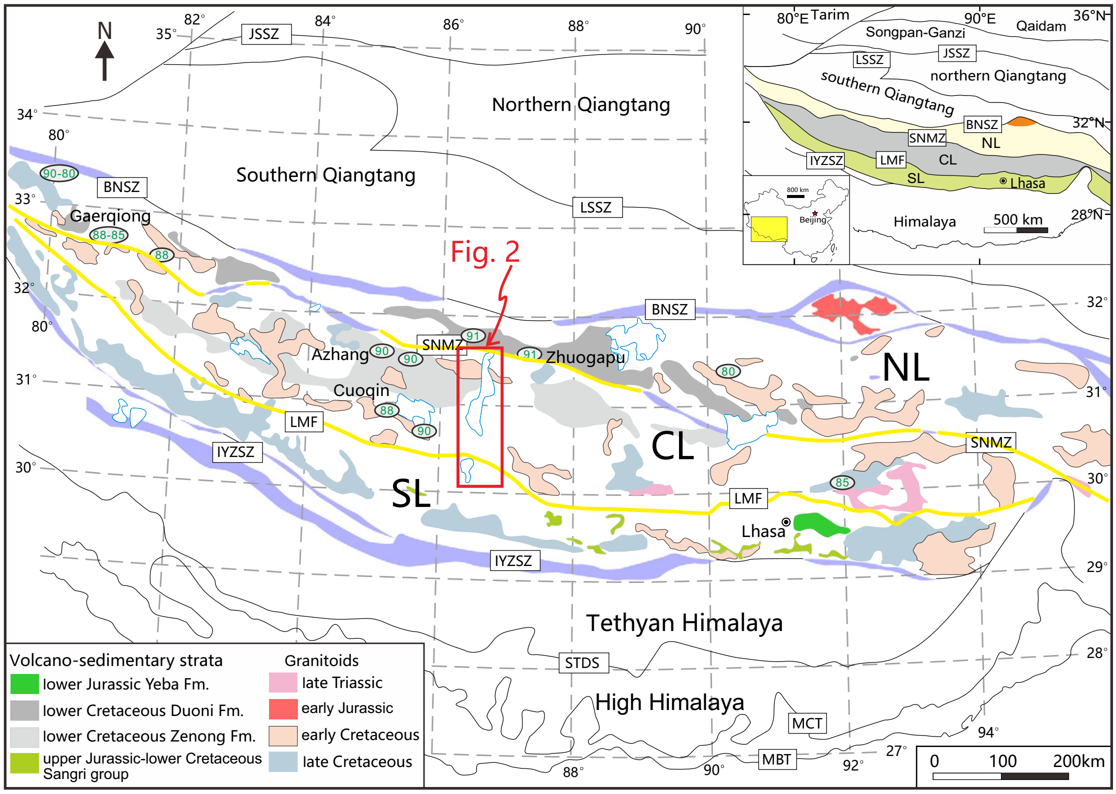
N
Northern Qiangtang
Southern Qiangtang
JSSZ
BNSZ
LSSZ
SNMZ
LMF
IYZSZ
STDS
MCT
MBT
Fig. 2
Gaerqiong
Azhang
Cuoqin
Zhuogapu
Lhasa
NL
CL
SL
Tethyan Himalaya
High Himalaya
Tarim
Songpan-Ganzi
Qaidam
northern Qiangtang
southern Qiangtang
Himalaya
500 km
Beijing
Volcano-sedimentary strata
lower Jurassic Yeba Fm.
lower Cretaceous Duoni Fm.
lower Cretaceous Zenong Fm.
upper Jurassic-lower Cretaceous Sangri group
Granitoids
late Triassic
early Jurassic
early Cretaceous
late Cretaceous
0 100 200km

Figure 2

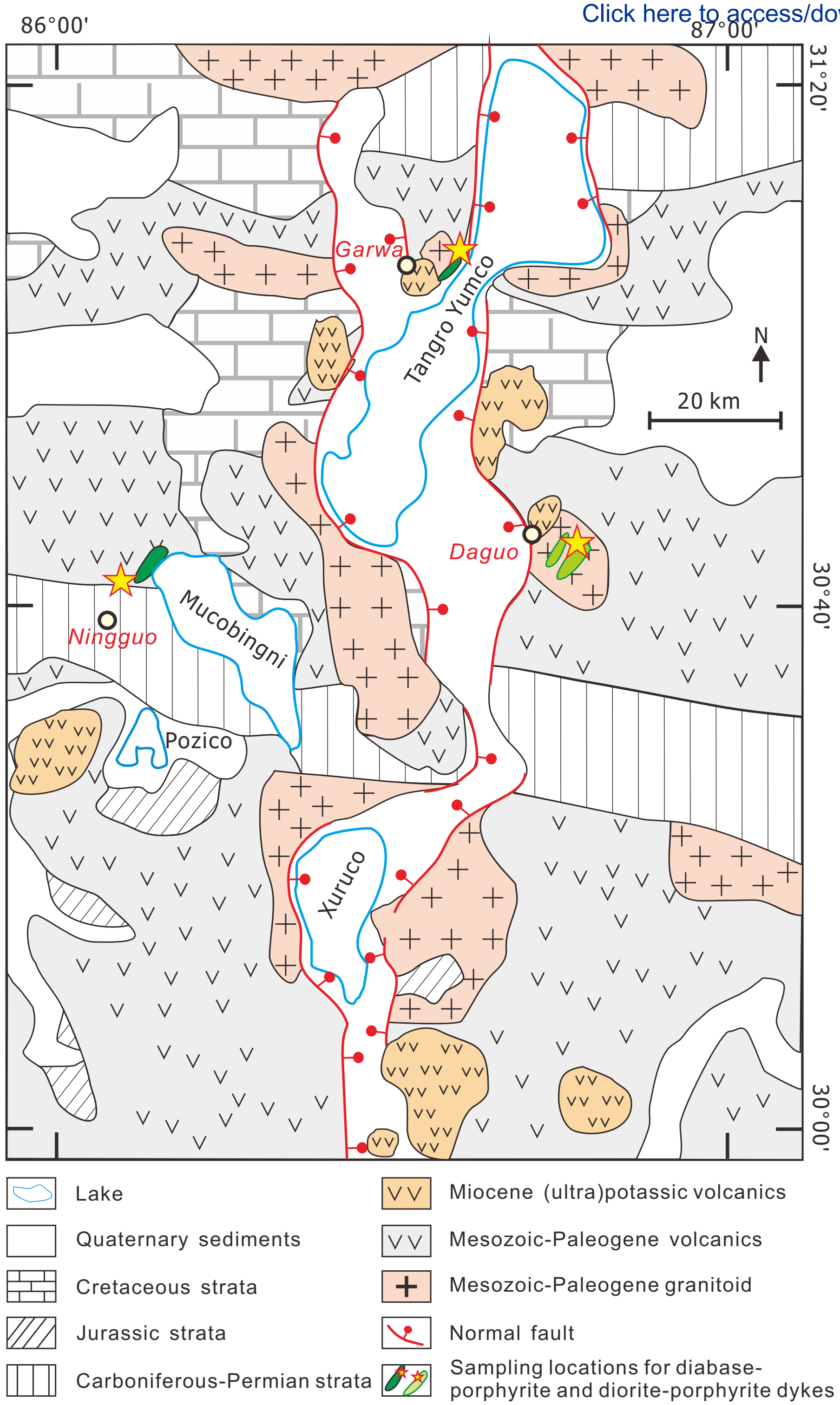

86°00'
87°00'
31°20'
30°40'
30°00'
N
20 km
Garwa
Tangro Yumco
Daguo
Ningguo
Mucobingni
Pozico
Xuruco
Lake
Quaternary sediments
Cretaceous strata
Jurassic strata
Carboniferous-Permian strata
Miocene (ultra)potassic volcanics
Mesozoic-Paleogene volcanics
Mesozoic-Paleogene granitoid
Normal fault
Sampling locations for diabase-porphyrite and diorite-porphyrite dykes

Figure 3

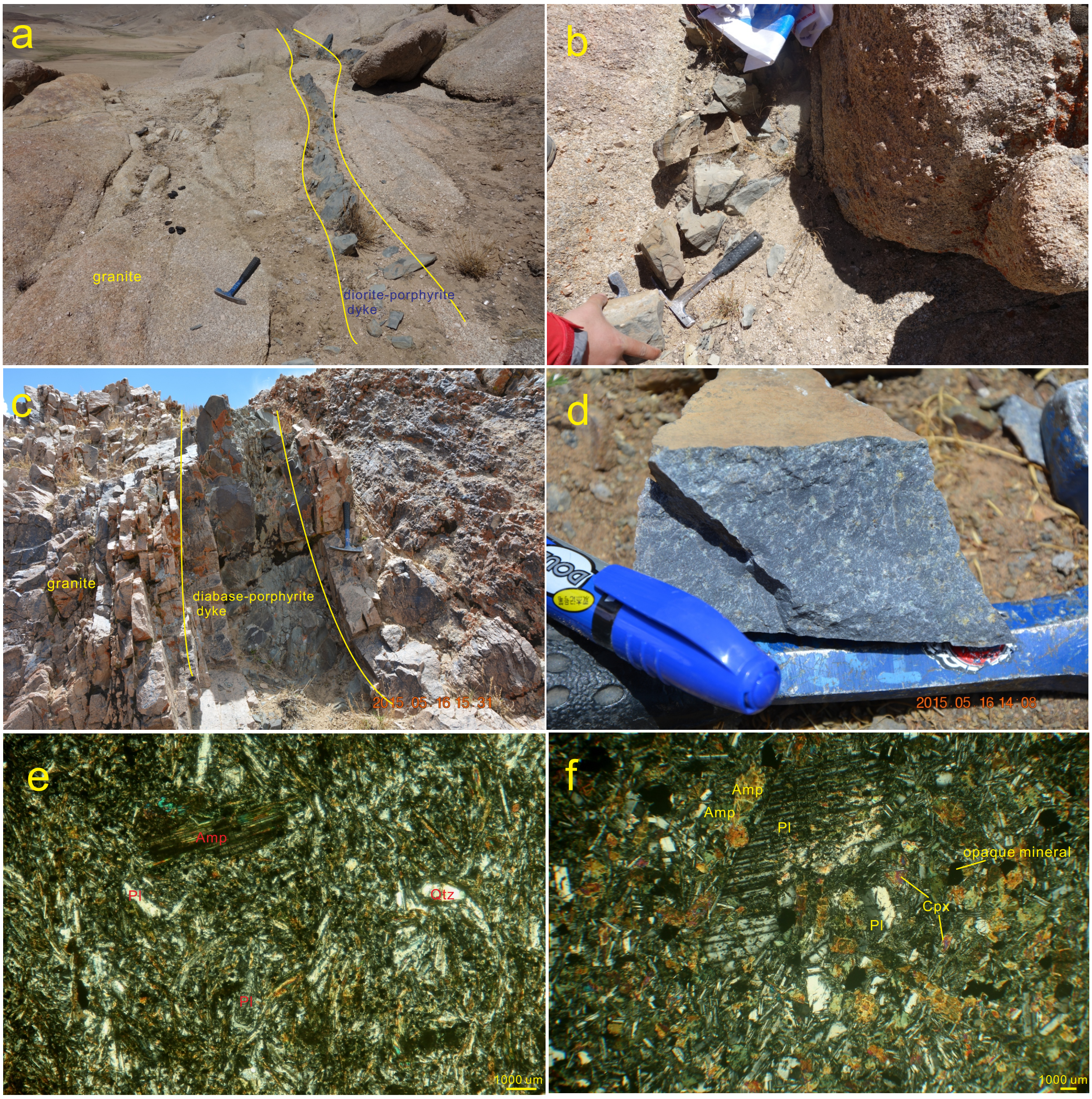
a
granite
diorite-porphyrite
dyke
b
c
granite
diabase-porphyrite
dyke
2015 05 16 15 31
d
2015 05 16 14 08
e
Amp
Pl
Qtz
Pl
1000 um
f
Amp
Amp
Pl
opaque mineral
Cpx
Pl
1000 um

Figure 4

Click here to access/download;Figure;Fig-4.pdf

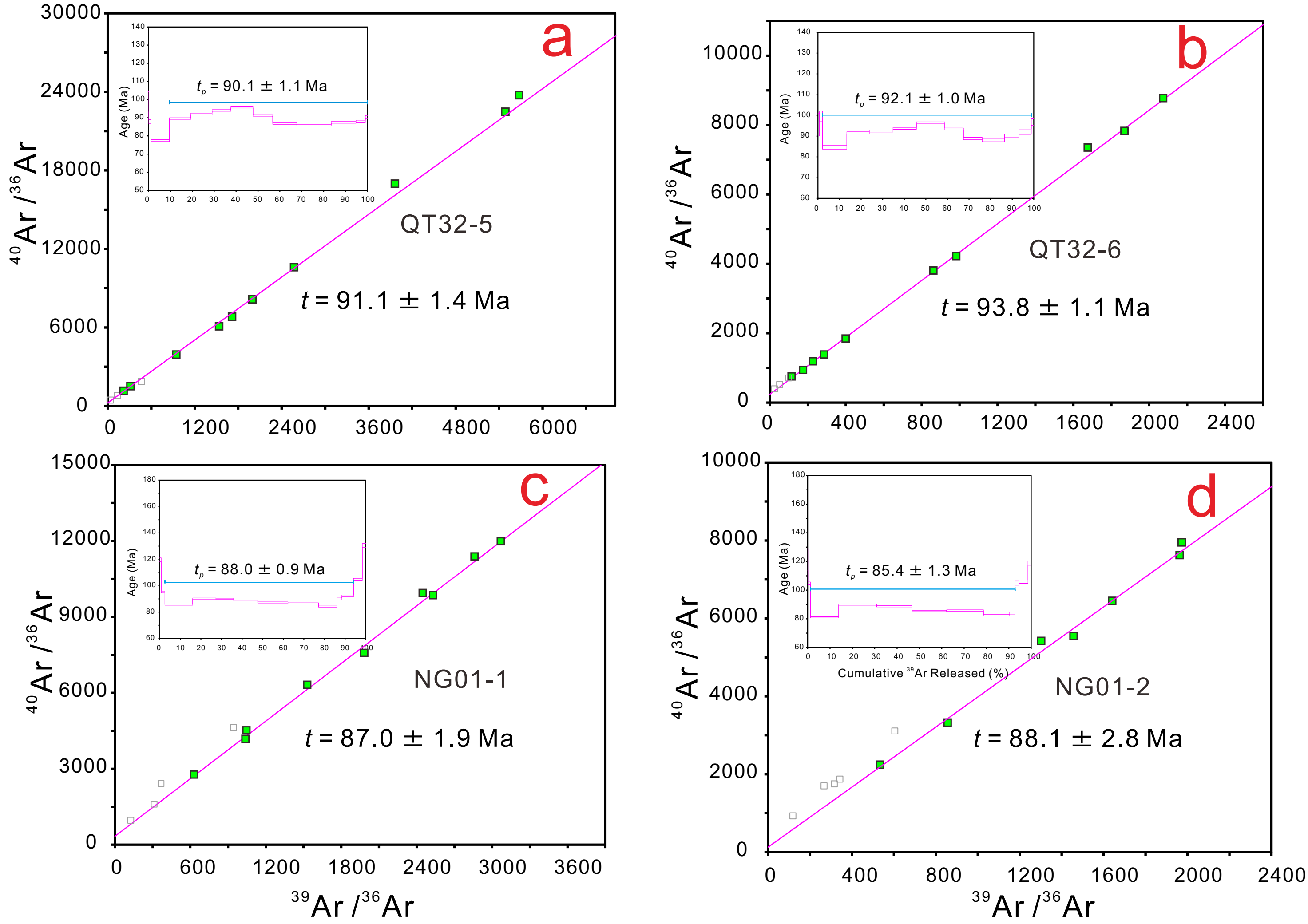

Figure 5

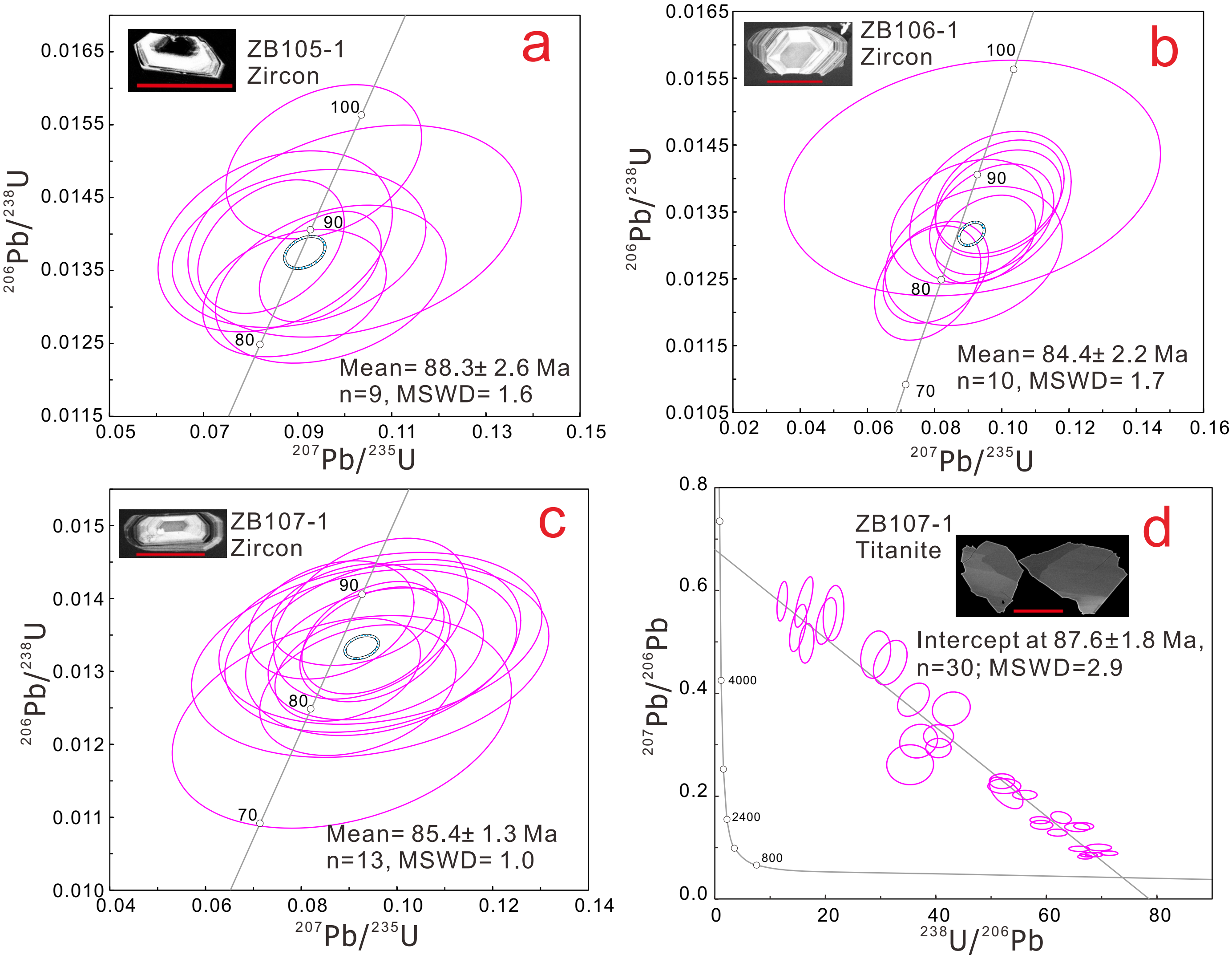
ZB105-1
Zircon
a
Mean= 88.3± 2.6 Ma
n=9, MSWD= 1.6
$^{206}Pb/^{238}U$
$^{207}Pb/^{235}U$
ZB106-1
Zircon
b
Mean= 84.4± 2.2 Ma
n=10, MSWD= 1.7
ZB107-1
Zircon
c
Mean= 85.4± 1.3 Ma
n=13, MSWD= 1.0
ZB107-1
Titanite
d
Intercept at 87.6±1.8 Ma,
n=30; MSWD=2.9
$^{207}Pb/^{206}Pb$
$^{238}U/^{206}Pb$

Figure 6

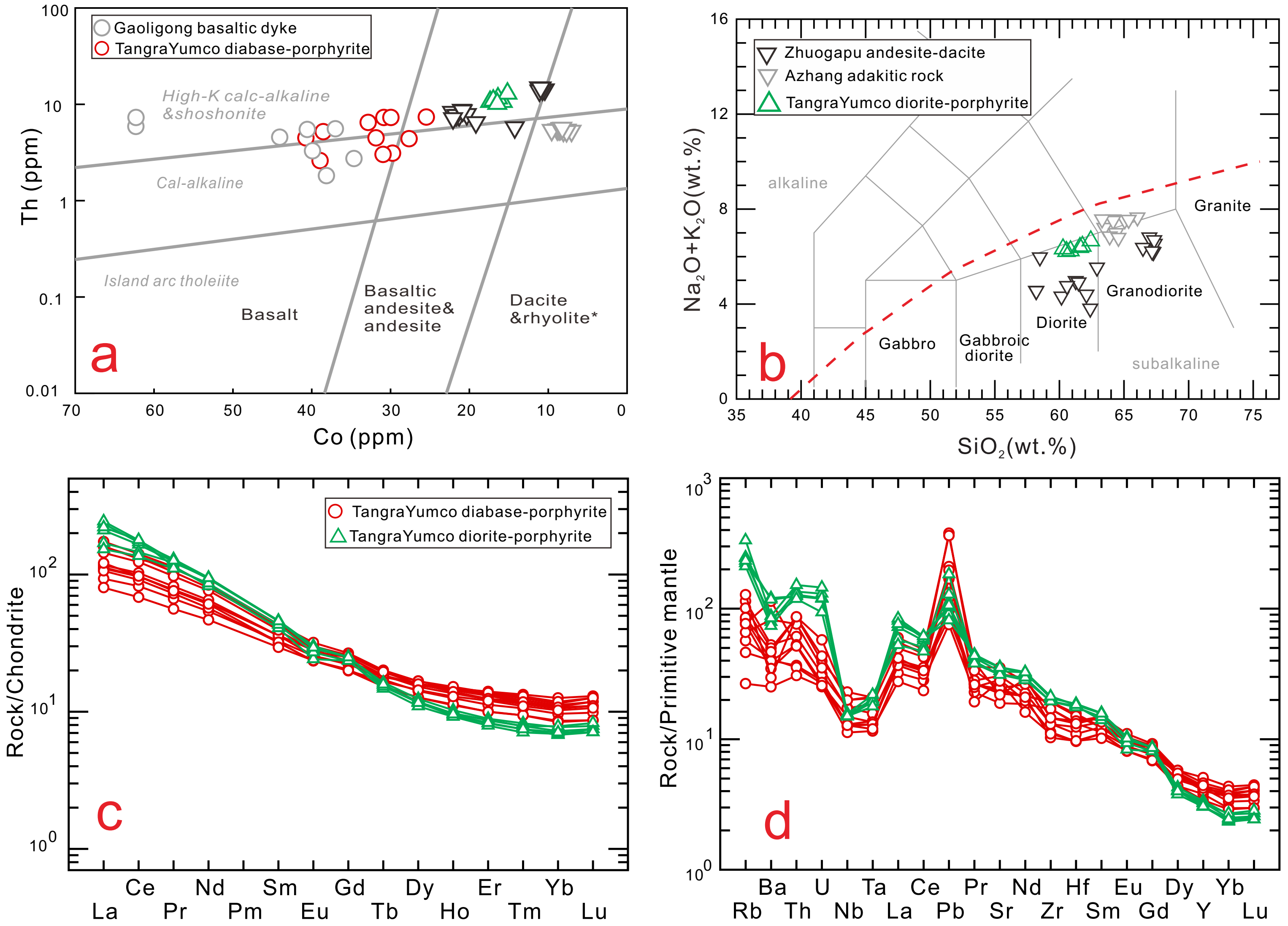

Gaoligong basaltic dyke
TangraYumco diabase-porphyrite
High-K calc-alkaline &shoshonite
Cal-alkaline
Island arc tholeiite
Basalt
Basaltic andesite& andesite
Dacite &rhyolite*
a
Th (ppm)
Co (ppm)
Zhuogapu andesite-dacite
Azhang adakitic rock
TangraYumco diorite-porphyrite
alkaline
Granite
Granodiorite
Diorite
Gabbro
Gabbroic diorite
subalkaline
b
Na_2O+K_2O(wt.%)
SiO_2(wt.%)
TangraYumco diabase-porphyrite
TangraYumco diorite-porphyrite
c
Rock/Chondrite
La Ce Pr Nd Pm Sm Eu Gd Tb Dy Ho Er Tm Yb Lu
d
Rock/Primitive mantle
Rb Ba Th U Nb Ta La Ce Pb Pr Sr Nd Zr Hf Sm Eu Gd Dy Y Yb Lu

Figure 7

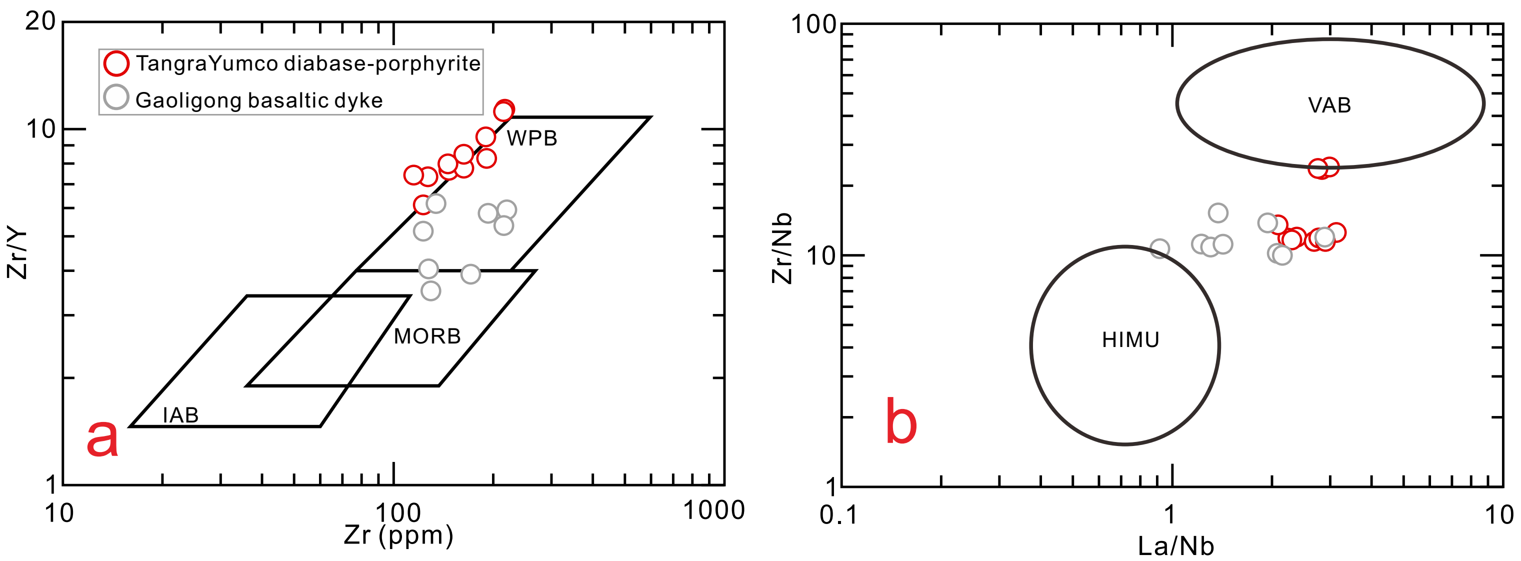

TangraYumco diabase-porphyrite
Gaoligong basaltic dyke
Zr/Y
Zr (ppm)
WPB
MORB
IAB
a
20
10
1
10
100
1000
VAB
HIMU
Zr/Nb
La/Nb
b
100
10
1
0.1
1
10

Figure 8

Click here to access/download;Figure;Fig-8.pdf

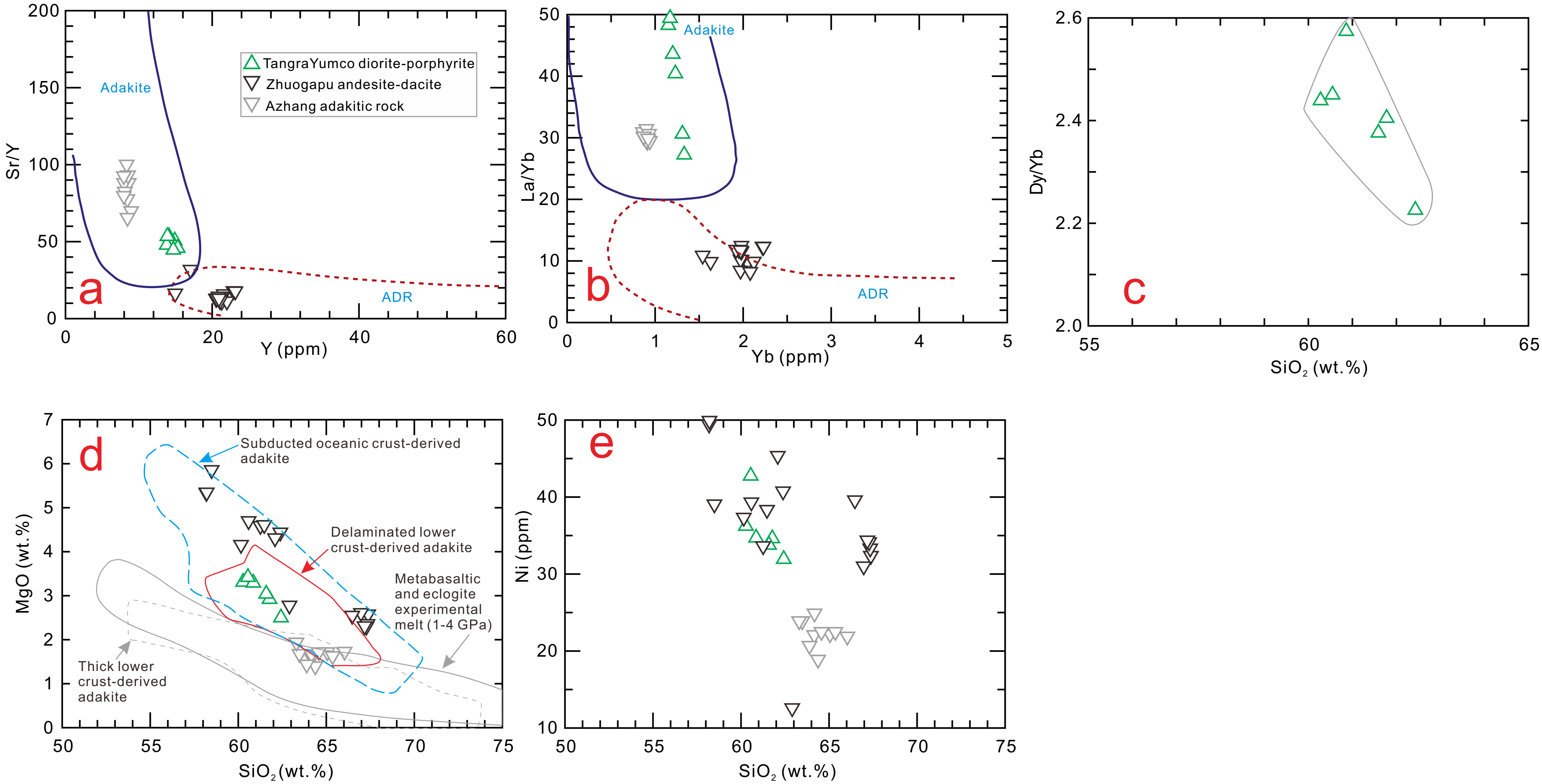

Figure 9

Click here to access/download;Figure;Fig-9.pdf

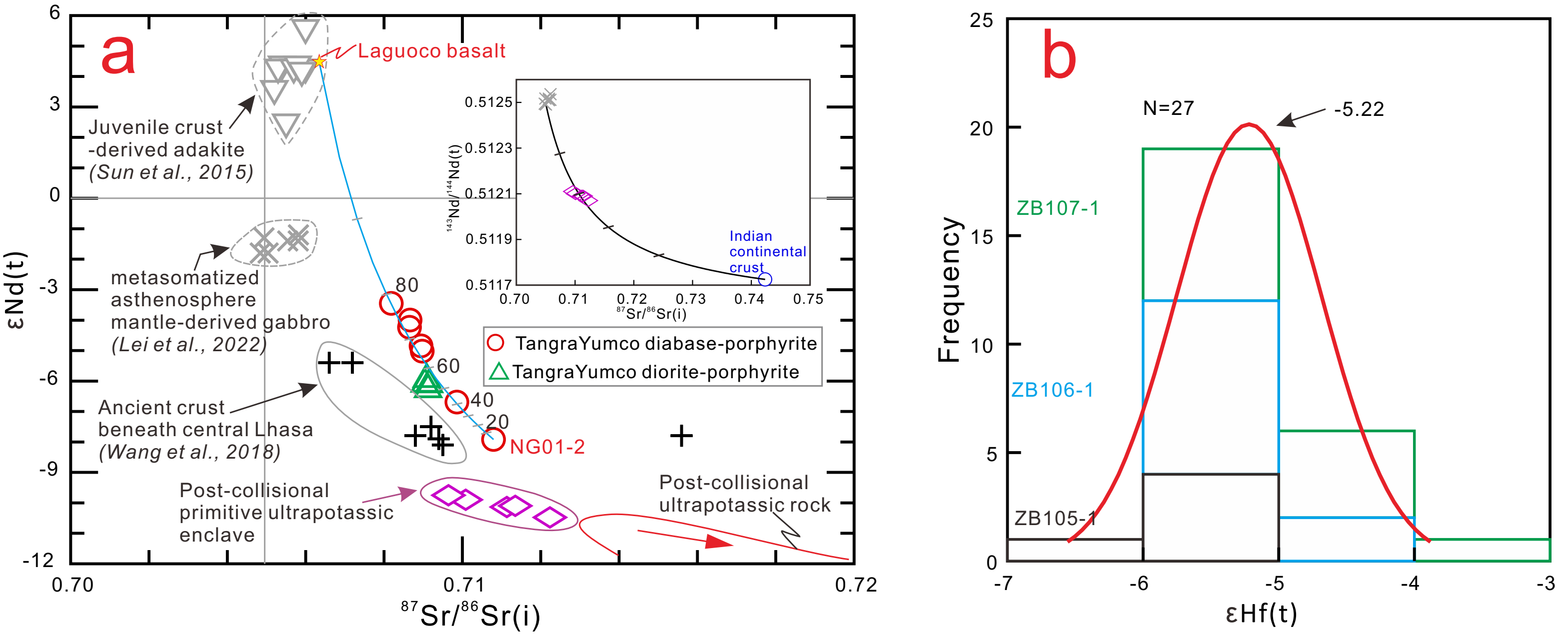

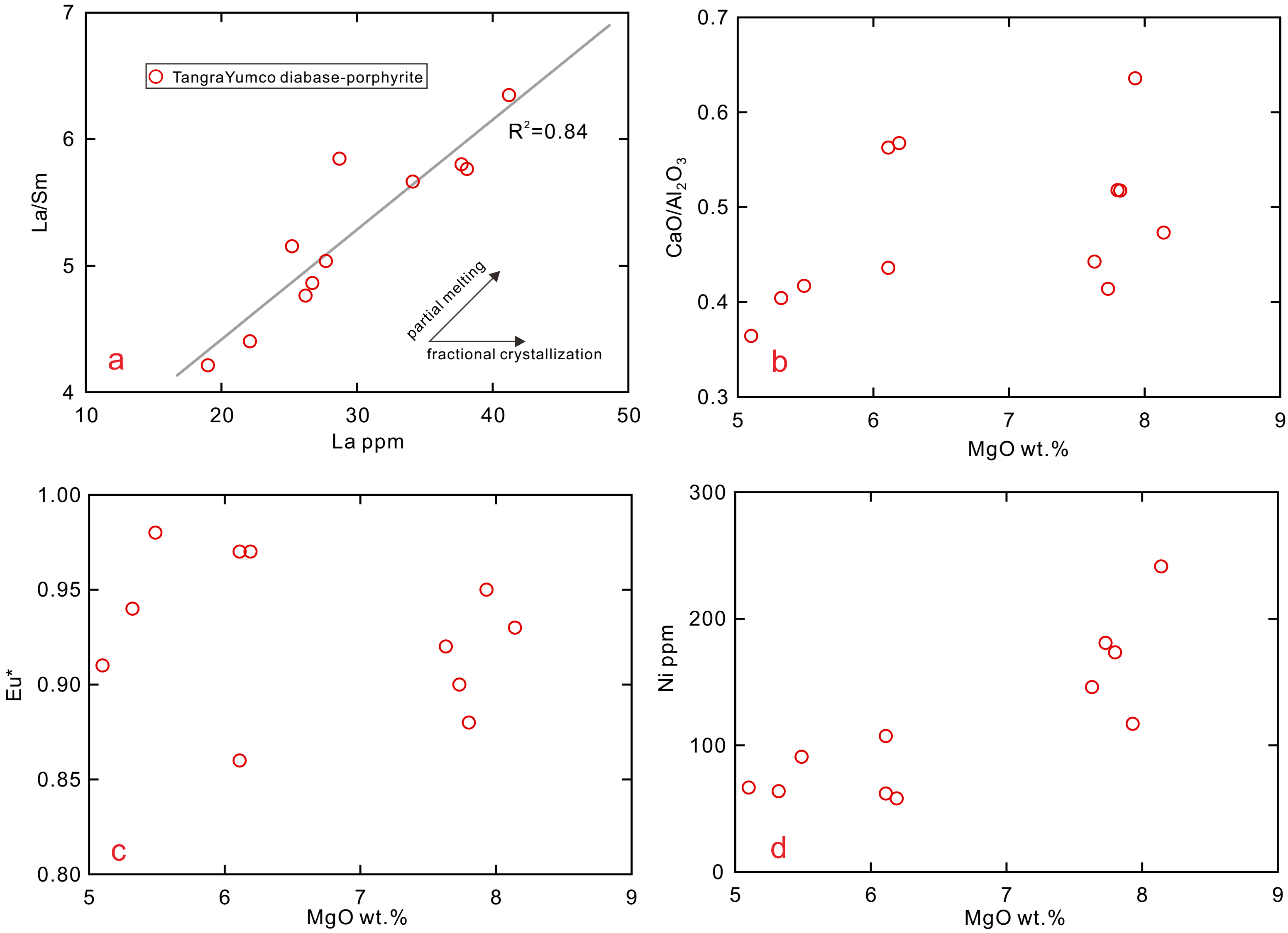

7
6
5
4
10
20
30
40
50
La/Sm
La ppm
TangraYumco diabase-porphyrite
R²=0.84
partial melting
fractional crystallization
a
0.7
0.6
0.5
0.4
0.3
5
6
7
8
9
CaO/Al2O3
MgO wt.%
b
1.00
0.95
0.90
0.85
0.80
Eu*
MgO wt.%
c
300
200
100
0
Ni ppm
MgO wt.%
d

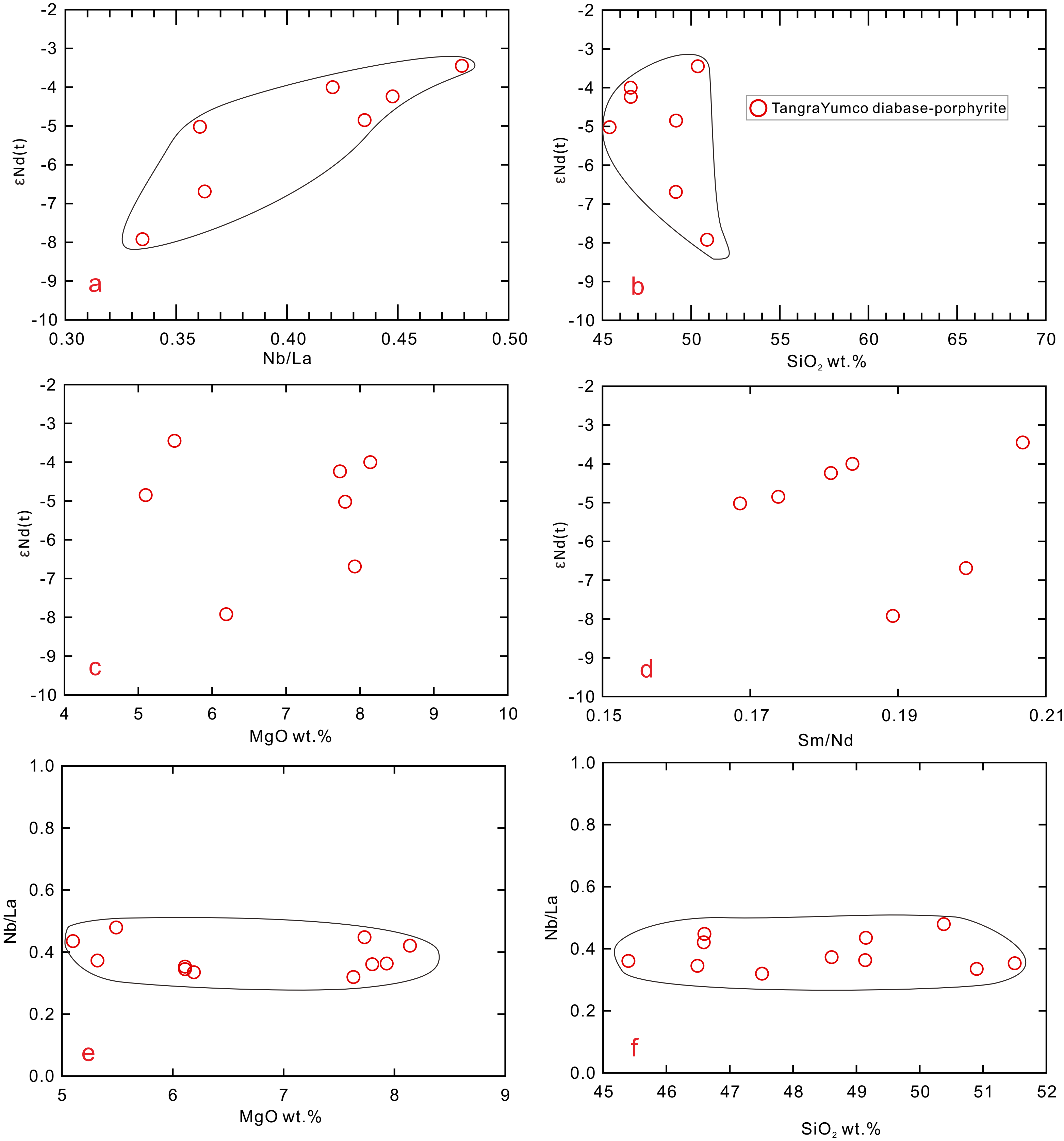

a
εNd(t)
Nb/La
0.30 0.35 0.40 0.45 0.50
-2 -3 -4 -5 -6 -7 -8 -9 -10
b
εNd(t)
SiO2 wt.%
45 50 55 60 65 70
TangraYumco diabase-porphyrite
c
εNd(t)
MgO wt.%
4 5 6 7 8 9 10
d
εNd(t)
Sm/Nd
0.15 0.17 0.19 0.21
e
Nb/La
MgO wt.%
5 6 7 8 9
1.0 0.8 0.6 0.4 0.2 0.0
f
Nb/La
SiO2 wt.%
45 46 47 48 49 50 51 52

Figure 12

Click here to access/download;Figure;Fig-12.pdf